



**HAL**  
open science

# Efficient polymerization and crystallization kinetics coupling of polyamide 6 synthesis for liquid composite molding process modeling

William Han, Quentin Govignon, Arthur Cantarel, Fabrice Schmidt

## ► To cite this version:

William Han, Quentin Govignon, Arthur Cantarel, Fabrice Schmidt. Efficient polymerization and crystallization kinetics coupling of polyamide 6 synthesis for liquid composite molding process modeling. Polymer Engineering and Science, In press, 10.1002/pen.25901 . hal-03563141v1

**HAL Id: hal-03563141**

**<https://imt-mines-albi.hal.science/hal-03563141v1>**

Submitted on 9 Feb 2022 (v1), last revised 21 Feb 2022 (v2)

**HAL** is a multi-disciplinary open access archive for the deposit and dissemination of scientific research documents, whether they are published or not. The documents may come from teaching and research institutions in France or abroad, or from public or private research centers.

L'archive ouverte pluridisciplinaire **HAL**, est destinée au dépôt et à la diffusion de documents scientifiques de niveau recherche, publiés ou non, émanant des établissements d'enseignement et de recherche français ou étrangers, des laboratoires publics ou privés.

# Efficient polymerization and crystallization kinetics coupling of polyamide 6 synthesis for liquid composite molding process modeling

William Han<sup>1</sup>  Quentin Govignon<sup>1</sup>  Arthur Cantarel<sup>2</sup>  Fabrice Schmidt<sup>1</sup> 

<sup>1</sup>Institut Clément Ader (ICA), Université de Toulouse, CNRS, IMT Mines Albi, INSA, ISAE-SUPAERO, UPS, Albi, France

<sup>2</sup>Institut Clément Ader (ICA), Université de Toulouse, CNRS, IMT Mines Albi, INSA, ISAE-SUPAERO, UPS, Tarbes, France

## Abstract

Variabilities in polyamide 6 (PA6) composite manufacturing by liquid processes can occur due to polymerization, crystallization, and flow through a fibrous preform. Numerical simulations of the process predicting the kinetics can facilitate manufacturing optimization. This study proposes an efficient modeling approach that can be integrated in current simulation discretization methods such as the finite volume method (FVM) while considering the interaction between PA6 polymerization and crystallization. Using polymerization and crystallization models issued from the literature, a previous study determined Hillier coupling method to be able to predict PA6 kinetics. A simpler and more efficient coupling will be introduced and adapted to account for process variability. It was integrated into an FVM framework for process simulation of injection showcasing the capabilities of the model to predict potential crystallization discrepancies.

## KEYWORDS

anionic polymerization, crystallization, injection molding, kinetics (polym.), modeling, reactive processing, simulations

## 1 | INTRODUCTION

Reactive thermoplastics systems have garnered attention because of their interesting advantages compared with molten thermoplastics. For instance, the reactive mix for polyamide 6 (PA6) synthesis boasts especially high fluidity at moderate temperatures (around 0.010–0.001 Pa.s below 473 K), contrasting with the very viscous molten PA6 needing higher temperatures (around 100–1000 Pa.s above 503 K).<sup>[1]</sup> This allows reactive thermoplastics systems to use liquid composite molding (LCM) processes that were traditionally restricted for thermoset composites processing. Notably, it makes possible to use the resin transfer molding (RTM) process for manufacturing thermoplastic composites with complex geometries and high production rates.<sup>[2]</sup> Moreover, synthesized thermoplastics

matrices keep the intrinsic advantages of thermoplastics when compared with thermosets as they can be further welded, repaired, and recycled.

With the right conditions, it has been observed that polymerization and crystallization can occur simultaneously during anionic polymerization of PA6 using a reactive mix.<sup>[3,4]</sup> Both phenomena affect the viscosity and the heat flux of the reactive system. Furthermore, their interaction is complex: while crystallization kinetics depends on how many polymer chains are available, it also favors lower temperatures. Thus, relative to the polymerization progress, crystallization occurs earlier and faster at lower temperatures; it is however tempered by a slower polymerization rate.<sup>[5]</sup>

To predict the thermoplastic composites' final properties after manufacturing, it is necessary to accurately

describe the PA6 synthesis. Additionally, the reactive mix flow during the RTM process is also a cause of variability throughout the manufactured component geometry, especially since a fibrous preform is involved.<sup>[6,7]</sup> Therefore, simulations of the kinetics during the manufacturing process allow to optimize cycle time and properties while limiting the need for costly experimental optimizations. Several frameworks for reactive simulation process have been proposed in the literature, coupling flow and polymerization<sup>[8–11]</sup> or more rarely flow and crystallization,<sup>[12]</sup> but to the best of the authors' knowledge, polymerization–crystallization coupled model for process simulation have rarely been proposed until now.

The global heat flow  $\varphi_s$  of the synthesis can be divided into the two principal phenomena occurring during the synthesis, namely polymerization and crystallization. Consequently, the usual strategy for modeling PA6 synthesis is to independently identify the polymerization heat flow  $\varphi_p$  and the crystallization heat flow  $\varphi_c$  (Equation 1).

$$\varphi_s(t) = \varphi_p(t) + \varphi_c(t) \quad (1)$$

Using thermograms obtained from PA6 synthesis with either the adiabatic reactor method or the differential scanning calorimetry (DSC) method, a first method to identify each phenomenon comes from Karger-Kocsis and Kiss.<sup>[13]</sup> It consists in mathematically separating the phenomena using two Gaussian curves and showed good fitting capabilities in recent studies conducted by Taki et al.<sup>[14]</sup> and Humphry et al.<sup>[15]</sup> However, while this method tacitly acknowledges polymerization influence on crystallization, the mathematical nature of the identification gives little insight on the nature of the coupling.

The first attempt found at describing the coupling between polymerization and crystallization comes from the analysis of coupled polymerization–crystallization realized by Korshak et al.<sup>[16]</sup> In their experiments, they isolated the polymerization contribution with a gravimetric study and observed that the conversion of polymerization and crystallization could be correlated using a piecewise linear function. Then Bolgov et al.<sup>[17]</sup> mentioned a more general approach, using kinetic models for the relative degree of conversion  $a$  (defined by Equation 2) and the relative degree of crystallinity  $b$  (Equation 3). These relative degrees describe the mass conversions ( $X_p(t)$ ,  $X_c(t)$ ) at a time, and are weighted by the total mass conversion at the end of the synthesis ( $X_p^\infty$ ,  $X_c^\infty$ ). They can also be calculated using the final enthalpies ( $\Delta H_p^\infty$ ,  $\Delta H_c^\infty$ ) and the heat fluxes ( $\varphi_p$ ,  $\varphi_c$ ). Thanks to Equation (4), they proposed a model for the reaction heat flow where the crystallization rate  $\dot{b}$  is linearly weighted by polymerization, therefore limiting crystallization to the polymerized portion of a sample. Then,

it was used by Malkin et al.<sup>[18]</sup> to describe PA6 synthesis, and later as a mean to determine crystallization kinetics by Lee et al.<sup>[19]</sup> and by Teuwen.<sup>[20]</sup>

$$a(t) = \frac{X_p(t)}{X_p^\infty} = \frac{1}{\Delta H_p^\infty} \int_0^t \varphi_p(x_t) dx_t \quad (2)$$

$$b(t) = \frac{X_c(t)}{X_c^\infty} = \frac{1}{\Delta H_c^\infty} \int_0^t \varphi_c(x_t) dx_t \quad (3)$$

$$\varphi_s(t) = \Delta H_p^\infty \dot{a}(t) + \Delta H_c^\infty (T) \dot{b}(t) a \quad (4)$$

In a recent work, Vicard et al.<sup>[21]</sup> worked at isotherms where crystallization and polymerization are decoupled in order to separately determine their respective kinetics. Therefore, the crystallization model was deduced from fully polymerized material and cannot be used without adjustment in Equation (1). In addition, Equation (4) was also unable to reconcile the polymerization model and the crystallization model. It is explained by the vastly different characteristic time of the two phenomena, which the decoupled crystallization model is unable to fully solve. Therefore, the modeled crystallization phenomenon ends prematurely, resulting in an incomplete description of the heat flow. To solve this problem, they used a customized Hillier coupling method (Equation 5) initially intended for describing primary and secondary crystallization<sup>[22]</sup> to determine the crystallization contribution to the synthesis of heat flow (Equation 6). It defines a local crystallization rate  $\frac{d\beta}{dx_t}$  unique to each new infinitesimal polymerized part of the reactive system. The global crystallization rate  $\dot{b}$  is subsequently calculated as the sum of the local crystallization kinetics of the reactive system polymerized part. To better resolve the different characteristic times inherent to polymerization and crystallization, Vicard et al. also added a diffusion factor  $f_d$  (Equation 7). It works as a corrector of how many newly formed polymerized chains can actually undergo crystallization and is inspired by the diffusion factor used in thermosetting curing models to account for vitrification influence on cross-linking kinetics.<sup>[23]</sup> The parameter  $C(T)$  determines the crystallization speed relative to polymerization, while  $D(T)$  determines the beginning of crystallization relative to polymerization.

$$\dot{b}(t, a) = \frac{d}{dt} \int_0^t (f_d^* a)(x_t) \frac{d\beta}{dx_t}(t - x_t) dx_t \quad (5)$$

$$\varphi_s(t) = \Delta H_p^\infty \dot{a}(t) + \Delta H_c^\infty \dot{b}(t, a) \quad (6)$$

$$f_d(t) = 1 - \frac{1}{1 + \exp(C(T)(a(t) - 1) + D(T))} \quad (7)$$

The distinctive part of this model is its convolution integral. To calculate the global crystallization rate, it

computes full crystallization kinetics for each newly infinitesimal polymerized part. This also means that only non-crystallized polymerized chains can undergo crystallization until the maximum crystallinity is locally reached, which is coherent with experimental observations. Another underlying hypothesis of this coupling is that existing crystals do not affect the crystallization kinetics of newly formed polymer chains. However, the presence of the convolution integral greatly complicates simulations. Indeed, to accurately calculate the convolution integral, the whole polymerization and crystallization history at every time step needs to be stored. This is computationally expensive and cannot be easily circumvented as discretizing the integral is complex to achieve even by resorting to linearization of the kinetic models.

The aim of this study is to propose a physically coherent coupling model, which is numerically efficient for process simulation, while keeping the synthesis description quality obtained from Vicard modeling. The polymerization and crystallization kinetic models parameters follow the identification conducted by Vicard et al.<sup>[21]</sup> on their experimental DSC curves obtained with the calorimetric method.<sup>[5]</sup> The Hillier coupling method is then compared with a new coupling approach. Afterward, few key parameters have been readjusted to account for the different modeling methods and more importantly, the variability of the experimental measurements. Finally, the model is integrated in OpenFOAM<sup>®</sup>, an open-source software, to compute an injection simulation where the influence of the reaction on the overall crystallinity is assessed.

## 2 | EXPERIMENTAL SYNTHESIS KINETICS

### 2.1 | Method

The PA6 synthesis is modeled using data obtained by Vicard et al. in their experimental study.<sup>[5]</sup> The reactants used for anionic PA6 synthesis came from components provided by Brüggemann Chemical, Germany, which are summarized in Table 1. The ratio of both the catalyst and the activator was defined at 0.79/1.10 mol% of the monomer.

The synthesis is characterized by its global heat flow  $\varphi$  [ $\text{Wg}^{-1}$ ], which was recorded by DSC at varying isotherms with a  $10^\circ$  interval between 403 K and 473 K. In Figure 1, one sample heat flow curve is shown for each isotherm tested, and separated between different behaviors. At 473 K, no crystallization peak is observed. It can be observed after the main peak at 463 K and 453 K before it starts coinciding with the main peak between

TABLE 1 Components of the PA6 reactive mix

Chemical compound	Function	Commercial name
$\epsilon$ -caprolactam	Monomer	AP-Nylon <sup>®</sup>
Caprolactam magnesium bromide	Catalyst	Nyrim C1 <sup>®</sup>
Bifunctional hexamethylene-1,6-dicarbamoylactam activator	Activator	Brüggolen C20P <sup>®</sup>

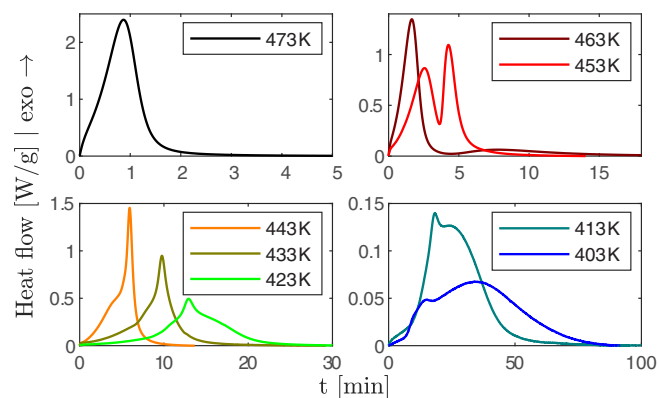


FIGURE 1 PA6 global synthesis kinetics measured in isothermal conditions using DSC

443 K and 423 K. Below 413 K, the crystallization peak happens before the main peak.

### 2.2 | Variability of the measurements

As observed in Figure 2, the DSC measurements show variable behavior in amplitude, which results in different durations for complete PA6 synthesis. The main cause for variability in measurements is thought to be residual humidity. Despite the care for reducing moisture uptake by drying reactive mix components and handling them in an inert atmosphere, the reactive mix has proved to be very sensitive to water. Indeed, Ueda et al.<sup>[24]</sup> and more recently, Wilhelm et al.<sup>[25]</sup> have observed that even a tenth of a percent of water content can significantly increase the synthesis duration. Other impurities can also negatively affect the synthesis speed.<sup>[3]</sup>

However, this variability in the shape of heat flow curve has little influence on the overall heat of reaction, as its value does not change in the same order of magnitude as the synthesis duration (see standard deviations [SD] in Table 2).

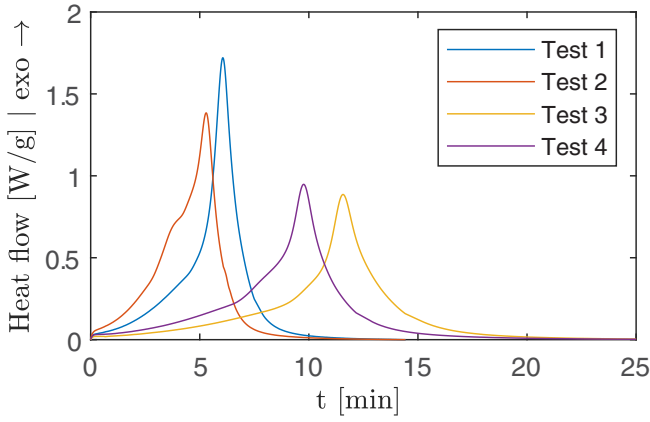


FIGURE 2 DSC measurements at 433 K

Moreover, since slowed-down polymerization is caused by parasite reactions, it can be assumed that causes of variability discussed above do not affect the intrinsic crystallization kinetics, as it is a phenomenon arising on already polymerized chains. Thus, the causes of the variability discussed above were assumed to mainly affect the reactivity and the polymerization rate. In subsequent modeling, a unified crystallization kinetics was also chosen. Therefore, it assimilates any secondary crystallization kinetics, which may be happening during the synthesis.<sup>[15,26]</sup>

### 3 | ISOTHERMAL SYNTHESIS MODELING

#### 3.1 | Basis

The aim is to model the global heat flow  $\varphi$  [ $\text{W g}^{-1}$ ] observed during PA6 synthesis. The total enthalpy of polymerization corresponds to the average total mass degree of conversion  $X_p^\infty$  measured ( $\overline{X_p^\infty} = 94.2 \pm 1.4 \text{ wt}\%^{[5]}$ ). The

crystallinity  $X_c$ , or mass degree of crystallization conversion, can be obtained with Equation (8) using the theoretical heat of fusion for a 100% crystalline PA6  $\Delta H_c^{100\%}$ , which is valued at  $230 \text{ J g}^{-1}$ .<sup>[27]</sup>

$$X_c(t) = \frac{\Delta H_c(t)}{\Delta H_c^{100\%}} \quad (8)$$

#### 3.2 | Polymerization modeling

In previous work by Vicard et al.,<sup>[21,26]</sup> the polymerization part of the reaction was modeled using Malkin and Camargo model,<sup>[28]</sup> which has been widely used to model the reactive PA6 kinetics. It is described by Equation (9), which consists in an Arrhenius law weighted by the influence of already polymerized material, which is characterized by the autocatalytic factor  $B_0$  and the reaction order  $n_p$ .

$$\dot{a} = A_p \exp\left(-\frac{E_a}{RT}\right) (1-a)^{n_p} (1+B_0 a) \quad (9)$$

The initial parameters used for this study are shown in Table 3 and had been determined at 463 K and 473 K, in which crystallization is minimal and mostly uncoupled with polymerization.

#### 3.3 | Crystallization modeling

The crystallization part of the reaction was modeled using Vicard et al. work.<sup>[21]</sup> The Nakamura model<sup>[29]</sup> was chosen, which extends the Avrami crystallization kinetics<sup>[30]</sup> for anisothermal conditions. It describes the evolution of the relative degree of crystallinity  $b$  following Equation (10) with  $n_c$  [-], the Avrami exponent distinctive of the crystals nucleation and growth and  $K_N$  [ $\text{s}^{-1}$ ], the Nakamura global kinetic constant. The latter was

TABLE 2 Total heat of reaction and crystallization enthalpy measured during the PA6 synthesis at different isothermal temperatures

Synthesis temperature $T_{\text{iso}}$ [K]	Total heat of reaction $Q_{\text{tot}}$ [ $\text{J g}^{-1}$ ]	SD of reaction heat [%]	Synthesis duration $t(Q(t) = Q_{\text{tot}})$ [min]	SD of synthesis duration [%]
403	$196.3 \pm 11.1$	5.7%	$109.1 \pm 27.4$	25%
413	$205.6 \pm 14.5$	7.0%	$73.0 \pm 16.5$	23%
423	$219.8 \pm 3.3$	1.5%	$28.0 \pm 1.9$	6.8%
433	$211.9 \pm 1.8$	0.9%	$19.1 \pm 7.6$	40%
443	$198.4 \pm 8.3$	4.1%	$16.1 \pm 5.7$	35%
453	$194.7 \pm 6.3$	3.2%	$8.4 \pm 0.4$	4.4%
463	$142.3 \pm 10.1$	7.1%	$22.3 \pm 2.7$	12%
473	$121.7 \pm 4.5$	3.7%	$8.8 \pm 6.0$	68%

TABLE 3 Parameters of Malkin and Camargo model

Parameters	Value	Unit
$A_p$	$1.34 \times 10^7$	$[\text{s}^{-1}]$
$E_a$	$9.15 \times 10^4$	$[\text{J mol}^{-1}]$
$B_0$	73.9	$[-]$
$n_p$	1.1	$[-]$

modeled with relation to temperature using the Hoffman–Lauritzen model.<sup>[31]</sup> According to Vicard et al.,<sup>[21]</sup> its advantage resides in taking both macromolecular diffusion and nucleation into account from the glass transition temperature to the equilibrium melting temperature. It is also consistent with PA6 spherulite growth observations by Magill<sup>[32]</sup> and with fast scan DSC measurements.<sup>[33,34]</sup> It follows Equation (11), in which  $U^*$ ,  $K_g$ , and  $T_\infty$  are parameters relative to macromolecular motion or crystallization growth, while  $T_m^0$  is the equilibrium melting temperature of PA6 crystals.

$$b = 1 - \exp\left(-\left(\int_0^t K_N T(x_t) dx_t\right)^{n_c}\right) \quad (10)$$

$$K_N = K_0 \exp\left(-\frac{U^*}{R(T - T_\infty)}\right) \exp\left(-\frac{K_g(T_m^0 + T)}{2T^2(T_m^0 - T)}\right) \quad (11)$$

A thermodependant induction time related to the equilibrium melting temperature  $t_{c,0}$  was also introduced using an equation similar to the Arrhenius law (Equation 12). It is similar to the characteristic crystallization time described by Bolgov et al.<sup>[17]</sup> and is highly dependent on the activator.

$$t_{c,0} = A_t \exp\left(\frac{E_t}{R(T_m^0 - T)}\right) \quad (12)$$

Hence, using the differential form of Equation (10), proposed by Patel et al.,<sup>[35]</sup> and taking the crystallization induction time into account, the Nakamura model is written following Equation (13), in which  $H$  defines the Heaviside function.

$$\dot{b} = H(t - t_{c,0}(T)) K_N(T) (1 - b) n_c \left[ \ln\left(\frac{1}{1 - b}\right) \right]^{\frac{n_c - 1}{n_c}} \quad (13)$$

To identify the model parameters, Vicard et al.<sup>[21]</sup> observed that at 453 K and 463 K, DSC curves of full PA6 synthesis were divided into two spikes, with the second corresponding to DSC curves from crystallization obtained by rapid cooling of melted PA6 samples

TABLE 4 Parameters of Nakamura–Hoffman–Lauritzen model<sup>[21]</sup>

Parameters	Value	Unit
$n_c$	1.59	$[-]$
$K_0$	$1.34 \times 10^7$	$[\text{s}^{-n_c}]$
$K_g$	$9.15 \times 10^4$	$[\text{K}^2]$
$U^*$	6300	$[\text{J mol}^{-1}]$
$T_\infty$	293.15	$[\text{K}]$
$T_m^0$	533.15	$[\text{K}]$
$A_t$	$5.17 \times 10^{-2}$	$[\text{s}^{-1}]$
$E_t$	$4.45 \times 10^3$	$[\text{J mol}^{-1}]$

at these temperatures. Therefore, the model was identified from DSC of PA6 crystallization obtained from molten PA6 and cooled from temperatures between 453 K and 463 K at  $-150^\circ/\text{min}$ . Their parameters are detailed in Table 4.

## 4 | COUPLING MODELING

The crystallization model presented earlier have been developed to describe crystallization occurring in polymers from the molten state.<sup>[21,29]</sup> With the right conditions, crystallization can occur simultaneously with polymerization during the synthesis.<sup>[19,36]</sup> Hence, it needs to be adapted for crystallization occurring during PA6 synthesis.

### 4.1 | An improved coupling model for curing simulations

As the high complexity of Vicard's coupling (Equation 5) contrasts with the simplicity of the other coupling methods, steps were taken to try and take the best parts of all coupling methods.

The first modification comes from the observation that Vicard's interpretation of Equation (4) has polymerization affecting only the heat flow of crystallization and not crystallization itself. For crystallization to be properly limited by polymerization, it has to be included directly in the crystallization model, similarly to what has been done with Hillier coupling and to what was implicitly done in most literature attempts of modeling coupled crystallization.<sup>[13–15,19,37]</sup>

Then, the polymer availability degree  $a_a$  is introduced in Equation (14), which depends on polymerization and previously defined parameters: the diffusion factor  $f_d$  and the crystallization induction time  $t_{c,0}$ . As its name



implies, it describes the amount of polymer chains available for crystallization.

$$a_a(t) = H(t - t_{c,0}(T))(f_d * a)(t - t_{c,0}(T)) \quad (14)$$

In order to strictly limit the crystallization kinetics to the polymer chains that can crystallize, the local degree of crystallization  $\beta$  is calculated using Equation (15). It hypothesizes that the local degree of crystallization is equal to the ratio between the global degree of crystallization and the polymerized chains available for crystallization at a point of time.

$$\beta(t) = \frac{b(t)}{a_a(t)} \quad (15)$$

Finally, this allowed the authors to propose a new general model to describe crystallization (Equation 16) during PA6 synthesis (Equation 17). Thus, similarly to Vicard et al. coupling,<sup>[21]</sup> a local crystallization rate is considered following Nakamura's model. However, contrary to Hillier formulation, the local crystallization degree is considered uniform within the polymerized part. Then, the local crystallization rate is weighted by the polymer availability degree to find the global crystallization rate, similarly to Bolgov et al. approach.<sup>[17]</sup>

$$\dot{b} = a_a H(t - t_{c,0}(T)) K_N(T) (1 - \beta) n_c \left[ \ln \left( \frac{1}{1 - \beta} \right) \right]^{\frac{n_c - 1}{n_c}} \quad (16)$$

$$\varphi(t) = \Delta H_p^\infty \dot{a}(t) + \Delta H_c^\infty(T) \dot{b}(t, a_a) \quad (17)$$

To compare the new coupled crystallization model (Equation 16) with the Hillier coupled crystallization (Equation 5), the crystallization rate was calculated using both methods with parameters in Tables 3 and 4 with no diffusion factor ( $f_d = 1$ ). In Figure 3, the results from the two models give very similar curves at 443 K and 463 K, with a difference in time span and amplitude at 453 K. The similar shapes are expected as the models have the same core principle, which is considering that only a part of already polymerized materials can be crystallized until they reach their maximum crystallinity. The difference lies in how the local crystallization kinetics are considered within the polymerized part. In Hillier coupling, the local crystallization kinetics depends on the polymerization history in each infinitesimal part of the polymerized phase in the reactive system. However, with Equation (16), the local crystallization kinetics depends instead on the crystalline phase density relatively to the polymerized part of the reactive system. Hence, unlike Hillier coupling that considers independence between crystallization kinetics of each infinitesimal polymerized

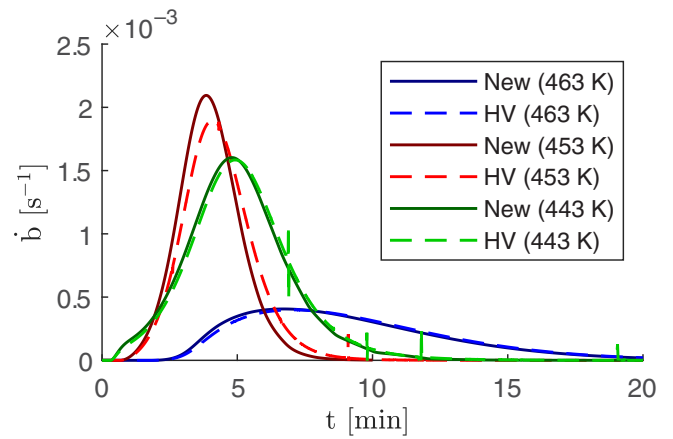


**FIGURE 3** Comparison between the crystallization rates with relation to time from the new crystallization coupled method (Equation 16) and Hillier-Vicard (HV) coupling method (Equation 5) at three isotherm values (443 K, 453 K, and 463 K)

part, the new coupling method considers that each new polymerized chain will feed the ongoing global crystallization kinetics, thus assuming that already existing crystals affect the crystallization kinetics. The difference at 453 K is explained by comparing the time span of crystallization of bulk polymer and the time span of polymerization. According to Vicard et al.<sup>[5]</sup> interpretation of DSC curves, when the temperature is low, polymerization is slow compared with the crystallization speed of polymer chains. Instead, at 463 K and higher, not only crystallization is a slow process, but because of the crystallization initiation time, it starts when polymerization is ending. Therefore, it is around 453 K that the difference of coupling methodology is most noticeable, as at this temperature polymerization and crystallization kinetics have both similar timespans and overlapping timeframes.

Because of the similar results given by the two methodologies, and since both need a corrective factor to limit polymer chain availability, the closest approach to reality was not identified. However, the new coupling method only uses simple calculations and differential equations, which greatly simplify its integration for simulations compared with the Hillier coupling method.

## 4.2 | Determination of new parameters for the coupling model

The parameters of the Malkin and Camargo model and the diffusion factor have been re-identified to better fit the new coupling model, and to take into account the variability in DSC measurements. In this following section, the procedure developed to identify the parameters for simulation is described.

## 4.2.1 | Choice of parameters optimization

### *Polymerization model*

To take into account the variability of the polymerization rate, at least one parameter in the Malkin and Camargo model has to be adapted accordingly. As the model is phenomenological in nature,<sup>[28]</sup> with its parameters being determined purely numerically using experimental results,<sup>[26]</sup> they are no evident parameters to choose. Recently, Wendel et al.<sup>[38]</sup> attempted to take humidity into account in a polymerization model for anionically synthesized PA6. They chose to modify parameters  $A_p$  and  $n_p$  and exponentially relate them to the number of reactive molecules according to time. Choosing to modify  $A_p$  concurs with a relatively linear-looking variation of the curve shape. On the other hand, their model of  $n_p$  showed very little variation throughout their test cases, so it has been considered constant in the following optimization. The activation energy  $E_a$  works as an indicator of  $A_p$  thermodependence and should therefore be modified only if a thermodependant variability is observed.

Nonetheless the autocatalytic parameter  $B_0$  was modified instead as it has a quasi-linear effect on the curve, which showed a very slight improvement in model fitting compared with  $A_p$  as shown in Figure 4. It also had the advantage to eventually let us switch to a Kamal–Sourour model type, which was successfully used to model PA6 synthesis<sup>[20]</sup> if results of  $B_0$  showed an Arrhenius-like thermal dependency.

Two parameters have been added in the polymerization model used for curve-fitting (Equation 18): an initial state of polymerization  $a_i$ , and an induction time  $t_i$ . They respectively aim to take into account eventual polymerization that occurred during the samples preparation, and intermediate reactions able to delay the reaction.<sup>[39]</sup> Finding the best fit for these two parameters alongside  $B_0$

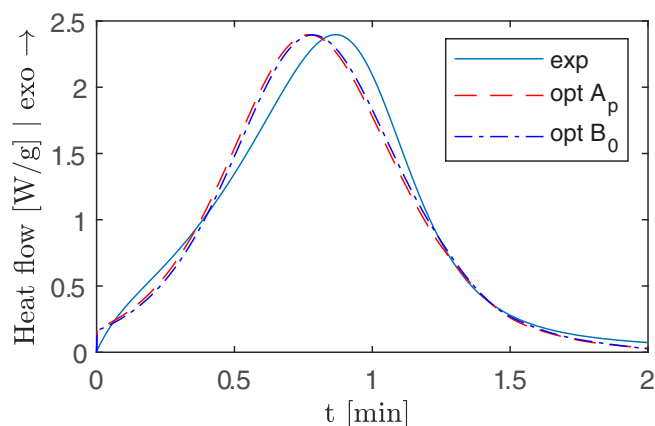


FIGURE 4 Comparison of  $A_p$  and  $B_0$  optimization for a DSC measurement at 473 K

aims to adapt the model to the sample properties as the cause for variability has not been formally identified.

$$\dot{a} = H(t - t_i)A_p(1 - a)^{n_p}(1 + B_0a)\exp\left(-\frac{E_a}{RT}\right)$$

$$a(t=0) = a_i \quad (18)$$

### *Crystallization model*

Following the observations made in Section 2.2, parameters of the Nakamura–Hoffman–Lauritzen model (Equation 13) identified by Vicard et al.<sup>[21]</sup> were used. However, the diffusion factor  $f_d$  (Equation 7) will be determined for each measurement because of the new coupling method.

## 4.2.2 | Optimization method

Determination of the model parameters has been conducted using MATLAB® Optimization Toolbox™ and MATLAB® Global Optimization Toolbox. It was observed that iterative methods such as the quasi-Newton method or the least square method tend to get trapped in local minima when working with the crystallization peak, presumably because of nonlinearities and Heaviside function usage. Consequently, when these local minima needed to be avoided, the pattern search method was preferentially used to minimize constrained objective functions. When possible,  $B_0$  was determined using the polymerization dominant spike by comparing the maximum heat flow at the relevant time using the half-time of the synthesis  $t_{50\%}$  ( $Q(t_{50\%}) = 0.5 * Q_{tot}$ ). Then  $t_i$  and  $a_i$  were obtained by minimizing the difference between the experimental and the simulated enthalpy at each point of the reaction. It was determined alongside  $B_0$  if only one reaction peak was visible (at 423 K, 433 K, and 443 K). Finally, the parameters  $C$  and  $D$  were obtained by minimizing the enthalpies differences with constraints to satisfy  $f_d(0.001, T) = 0$  and  $f_d(0.999, T) = 0$ . Parameters of the coupling model were taken from Vicard<sup>[26]</sup> and used as initial guesses for  $B_0$ ,  $C$ , and  $D$ , while initial guesses for  $t_i$  and  $a_i$  were zero. The optimization procedures are summarized in Figure 5 and were conducted for each experimental DSC measurement.

## 4.2.3 | Optimization method and results

Mean value and extrema for parameter optimization for the polymerization part of the curve are presented for  $B_0$ ,  $a_i$ , and  $t_i$  in Table 5. Because of the high discrepancies



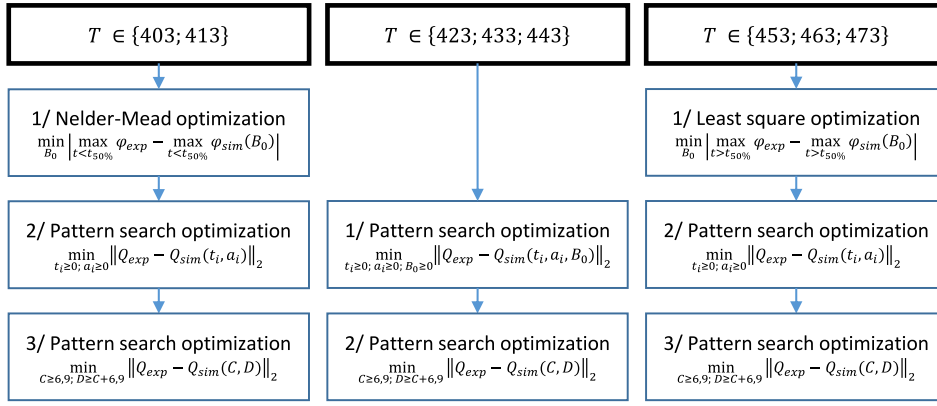


FIGURE 5 Model optimization method depending on temperature

Parameters	Value	Unit	Maximum	Minimum
$B_0$	$88.21 \pm 28,17$	[-]	154.51	34.02
$a_i$	$0.0130 \pm 0.0151$	[-]	0.0604	0
$t_i(T \geq 453 \text{ K})$	$1.04 \pm 1.79$	[s]	5.0	0
$t_i(T < 453 \text{ K})$	$50.2 \pm 63.1$		151	0

TABLE 5 Mean value and extrema of  $t_i$ ,  $a_i$  and  $B_0$

TABLE 6 Interpolation of C and D from optimization results

Temperature range	C and D expression	$f_d$
$T < 423 \text{ K}$	$C(T) = \exp(2.125 * 10^{-3} T^2 - 0,2541T + 72.30)$ $D(T) = \exp(-1.119 * 10^{-3} T^2 - 0,8889T - 160,5)$	Equation (7)
$T \in [423 \text{ K}, 463 \text{ K}]$	$C(T) = \exp(7.739 * 10^{-6} T^4 - 0,01342T^3 + 8.728T^2 - 2.522 * 10^3 T + 2.733 * 10^5)$ $D(T) = \exp(5,320 * 10^{-6} T^4 - 9.258 * 10^{-3} T^3 + 6,042T^2 - 1.753 * 10^3 T + 1.907 * 10^5)$	Equation (7)
$T > 463 \text{ K}$	-	$f_d = 1$

between values of  $t_i$  at higher and lower temperatures, two sets of values are presented.

For parameters  $C$  and  $D$ , the obtained values were interpolated using polynomials inside an exponential (Table 6, Figure 6). This choice was taken to ensure a smoother and more realistic interpolation than linear interpolation or polynomial interpolation, while mostly keeping the same monotonicity between points. As  $C$  and  $D$  reach very high values at 463 K, and because crystallization coupling becomes less relevant above 463 K, the diffusion factor was ignored at higher temperatures ( $f_d = 1$ ).

As Figure 7 shows with the optimization results for the slowest and fastest reaction in DSC tests, the optimization procedure is able to faithfully describe the heat flow caused from PA6 synthesis. However, the description of crystallization phenomenon tends to numerically average the heat flow integral and as such, description could still be improved, notably at 453 K. One possibility would be to take secondary crystallization into account, which would further complicate modeling, but improve

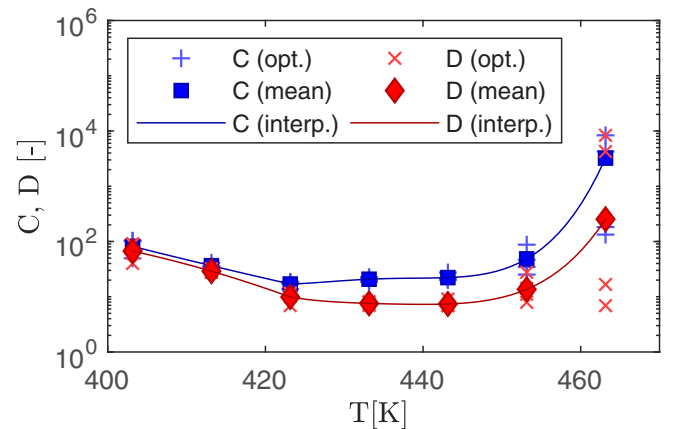


FIGURE 6 Interpolation described in Table 6 compared with optimized values, signaled with a sign, of  $C$  (+) and  $D$  (x) for each experimental DSC curves. The mean value at each isotherm is described by a square for  $C$  and a diamond for  $D$

description.<sup>[26]</sup> With the thicker curves, a common average model at 413 K, 433 K, and 453 K is showcased, which parameters use the mean values and expression

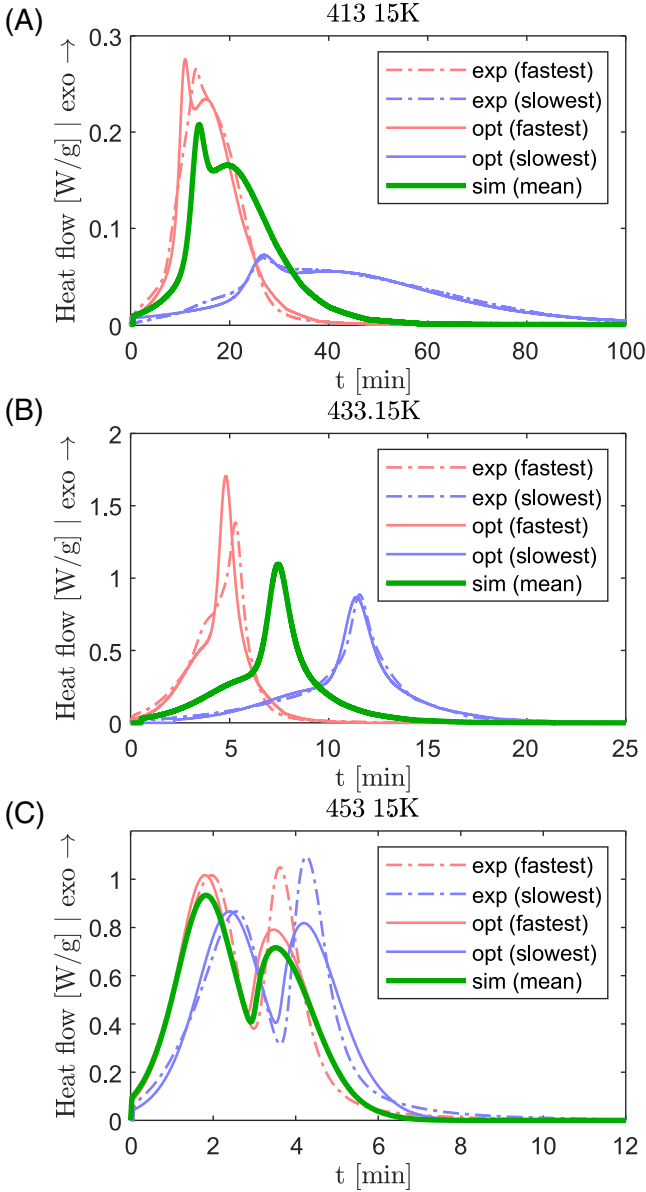


FIGURE 7 From top to bottom: DSC measurements compared with optimized model at 413 K, 433 K, and 453 K

TABLE 7 Total heat of reaction and crystallization enthalpy measured during the PA6 synthesis at different isothermal temperatures

Parameters	Value	Unit
$\Delta H_p^\infty$	116.3	[J g <sup>-1</sup> ]
$\Delta H_c^\infty(T)$		
$T \in [365.3 \text{ K}, 472.3 \text{ K}]$	$-0.0354T^2 + 29.651T - 6107.5$	[J g <sup>-1</sup> ]
$T \notin [365.3 \text{ K}, 472.3 \text{ K}]$	0	

presented in Tables 5 and 6, as well as the enthalpies determined from experimental values by Vicard et al.<sup>[5]</sup> detailed in Table 7. Because it takes the average of  $B_0$  at

all temperatures, it is as fast as the fastest synthesis at 453 K while it gives a good compromise at 413 K and 433 K.

## 5 | NUMERICAL SIMULATION

A numerical simulation of an injection of the reactive PA6 system has been developed using OpenFOAM<sup>®</sup>, an open-source computational fluid dynamics toolbox.

### 5.1 | PA6 flow modeling

A biphasic model is used to model the flow of the reactive mix in the air. It is based on continuity Equation (19) and momentum Equation (20) of the incompressible Navier–Stokes equations. The front is tracked using the volume of fluid (VOF) method (Equation 21) with an interface compression term.<sup>[40]</sup> In these equations,  $\mathbf{u}$  is the velocity field shared by both phases and  $p$  is the pressure.  $\eta$  and  $\rho$  are respectively the mixed dynamic viscosity and the mixed phase density in an element. Despite the reactive system density varying depending on its temperature and state (monomer, polymerized amorphous or crystalline),<sup>[26]</sup> a constant value has been chosen to keep the incompressible framework. The viscosity  $\eta_r$  is modeled using a phenomenological law, which relate viscosity to polymerization equation. It was experimentally determined by Davé et al.<sup>[41]</sup> and deemed accurate when  $a < 0.5$  (Equation 22).  $\eta_{r,0}$  (Equation 23) is calculated following an Arrhenius law determined in a previous work.<sup>[11]</sup> The influence of crystallization in viscosity is not taken into account.

$$\nabla \cdot \mathbf{u} = 0 \quad (19)$$

$$\rho \left( \frac{\partial \mathbf{u}}{\partial t} + \mathbf{u} \cdot \nabla \mathbf{u} \right) = -\nabla p + \eta \Delta \mathbf{u} \quad (20)$$

$$\frac{\partial \alpha_r}{\partial t} + (\nabla \cdot \mathbf{u}_r) \alpha_r + \nabla \cdot [(\mathbf{u}_r - \mathbf{u}_g) \alpha_r (1 - \alpha_r)] = 0 \quad (21)$$

$$\eta_r(t) = \eta_{r,0}(T) \exp(19.6 * a(t)) \quad (22)$$

$$\eta_{r,0}(T) = 8.123 * 10^{-7} \exp\left(\frac{3385}{T}\right) \quad (23)$$

The synthesis of PA6 is tracked using transport equations. First, polymerization is calculated both at  $t$  and  $t - t_{c,0}(T)$  with Equation (24). Crystallization is then calculated with Equation (25). The polymerization rate  $\dot{a}$  follows Malkin and Camargo model (Equation 9) while the crystallization rate  $\dot{b}$  follows Equation (16) with the

aforementioned and optimized parameters. The reaction heat flow is subsequently calculated following Equation (17) and the crystallinity is calculated following Equation (8). The singular points that can possibly occur in the crystallization equation are handled similarly to Levy's adaptation of crystallization kinetics.<sup>[42]</sup>

$$\frac{\partial a}{\partial t} + \nabla \cdot (\mathbf{u}a) = \dot{a} \quad (24)$$

$$\frac{\partial b}{\partial t} + \nabla \cdot (\mathbf{u}b) = \dot{b} \quad (25)$$

Then, heat Equation (26) is calculated with  $\kappa$  and  $c_p$  being respectively the thermal conductivity and the heat capacity of the mix. The variation of temperature  $T$  caused by PA6 synthesis, described by the source term  $\dot{q}$  (Equation 27), is calculated using the reaction enthalpy (Equation 17) and weighted by the amount of the reactive system  $\alpha_r$  (reactive mix + polymerized chain).

$$\frac{\partial T}{\partial t} + \nabla \cdot (\mathbf{u}T) - \frac{1}{\rho c_p} \nabla \cdot \kappa \nabla T = \dot{q} \quad (26)$$

$$\dot{q}(t) = \frac{\varphi_s(t)}{c_p} \alpha_r \quad (27)$$

Finally, if  $b < 1$ , the crystallization progress is updated following Equation (28) as to reflect the crystallization progress relative to the possible crystallization at the current simulated temperature.  $b$  is capped at 1 to signal when crystallization cannot progress anymore ( $\Delta H_c(t) \geq \Delta H_c^\infty(t)$ ).

$$b(t + \Delta t) = \frac{\Delta H_c^\infty(t)}{\Delta H_c^\infty(t + \Delta t)} b(t) \quad (28)$$

## 5.2 | Computational method

The PA6 synthesis kinetics equations have been implemented in OpenFOAM<sup>®</sup>. The Navier–Stokes equations are solved using the pressure implicit with splitting of operators algorithm (PISO): a segregated pressure–velocity solver for transient flows<sup>[43]</sup>. The kinetics transport equations are computed immediately afterward. In order to take the temperature dependence of final crystallinity, the degree of crystallization  $b$  is updated after solving the heat equation. The equations are discretized using the Finite volume method (FVM) with mostly second-order accurate schemes: the Crank–Nicolson scheme is used for time discretization and linear

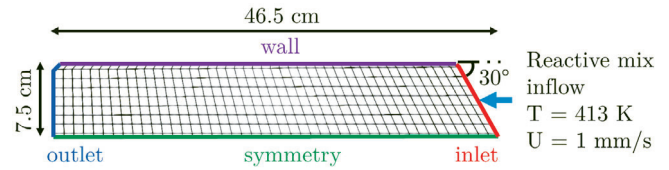


FIGURE 8 Description of the simulation geometry

differencing and linear upwind differencing are respectively used for the diffusion term, and the convection term in the Navier–Stokes equation. The Van Leer scheme<sup>[44]</sup> is used for advection terms in other transport equations. The time step is adjusted following a maximum Courant number chosen at 0.001 to ensure stability and accuracy (Equation 29).

$$Co = \frac{|\mathbf{u}| \Delta t}{\Delta l} < 0.001 \quad (29)$$

## 5.3 | Numerical simulation of a reactive mix injection

The flow domain describes a half of an adiabatic mold, which is a prism with a trapezoid base. It has an inlet boundary from where the reactive mix is injected, and an outlet boundary where air is subsequently expelled. It was meshed using 405 hexahedra with one element in the thickness to emulate a 2D simulation: the upper and lower face of the domain have symmetry boundary conditions. One face of the prism indicated in Figure 8 serves as a symmetry plane. Boundary conditions for the inlet, outlet, and other planes are indicated in Table 8 and describe an injection of a reactive mix at 413 K in an adiabatic domain. The geometry alongside the meshing is presented in Figure 8. The injection lasts 10 min, then the reactive mix inflow is stopped for 20 min to monitor the progress of the synthesis for an overall simulation time of 30 min. During this latter step, the Navier–Stokes equations (Equations 19 and 20) are not solved to avoid numerical instabilities.

## 5.4 | Results and discussion

During the injection, because of the constant reactive mix inflow, the front progresses mostly linearly (Figure 9). At the end of injection, the domain is 99.8% filled. As it is injected just mixed and unreacted, the reaction has progressed more at the front than at the inlet. Therefore, Figure 10A,B show that at the end of the injection, polymerization and crystallization has most

TABLE 8 Boundary conditions

Parameters	Inlet	Outlet	Wall
$U(t \leq 10 \text{ min})$	$0.001 \text{ m s}^{-1}$	$\frac{\partial U}{\partial n} = 0$	$U = 0$
$U(t > 10 \text{ min})$	$0 \text{ m s}^{-1}$		
$p$	$\frac{\partial p}{\partial n} = 0$	$10^5 \text{ Pa}$	$\frac{\partial p}{\partial n} = 0$
$\alpha_{i \in \{r,g\}}(t \leq 10 \text{ min})$	0	$\frac{\partial \alpha_i}{\partial n} = 0$	$\frac{\partial \alpha_i}{\partial n} = 0$
$\alpha_{i \in \{r,g\}}(t > 10 \text{ min})$	$\frac{\partial \alpha_i}{\partial n} = 0$		
$a(t \leq 10 \text{ min})$	0	$\frac{\partial a}{\partial n} = 0$	$\frac{\partial a}{\partial n} = 0$
$a(t > 10 \text{ min})$	$\frac{\partial a}{\partial n} = 0$		
$b(t \leq 10 \text{ min})$	0	$\frac{\partial b}{\partial n} = 0$	$\frac{\partial b}{\partial n} = 0$
$b(t > 10 \text{ min})$	$\frac{\partial b}{\partial n} = 0$		
$T(t \leq 10 \text{ min})$	413 K	$\frac{\partial T}{\partial n} = 0$	$\frac{\partial T}{\partial n} = 0$
$T(t > 10 \text{ min})$	$\frac{\partial T}{\partial n} = 0$		

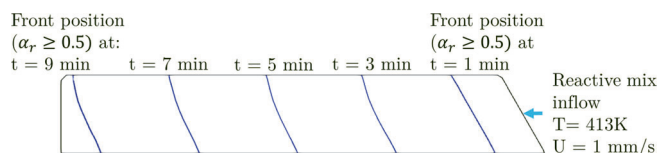


FIGURE 9 Reactive mix front position (determined at  $\alpha_r > 0.5$ ) at different time of the simulation

advanced near the outlet. Due to the initiation time, crystallization has not started in the inlet half of the domain, where the reactive mix is younger. Moreover, the temperature distribution in Figure 10C shows that following the start of the synthesis the temperature has already risen of few degrees but is lower at the corners of the outlet where some air is left.

In Figure 11, which describes the timeline of the proportion of fully polymerized and crystallized reactive mix in the domain, the synthesis has been fully completed in a substantial part of the domain as soon as 22.5 min passed since the injection beginning. Polymerization and crystallization were both completed in the whole domain after 30 min. Not only it is much faster than the isothermal synthesis model (in Figure 7 the simulated reaction lasts around an hour at 413 K), but the simulated crystallization finishes before polymerization. This means that the reaction has caused the temperature to reach a value at which crystallization cannot occur anymore.

It is confirmed by looking at the distribution of temperature shown in Figure 12. Looking at  $t = 20 \text{ min}$ , it can be observed that in the fully crystallized part, the temperature has reached 470 K at which crystallization is nearly nonexistent. Thus, looking at Figure 12C, the crystallinity reaches 18%, its maximum, which is far from the

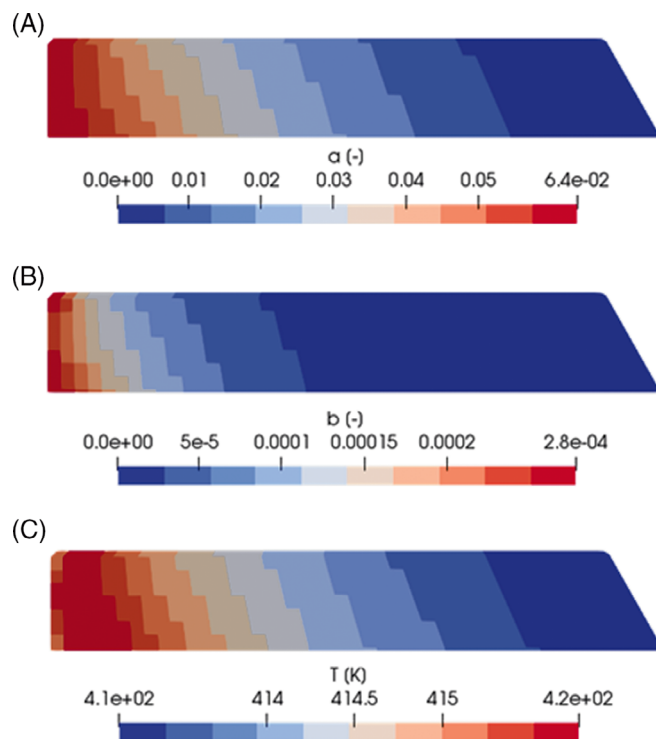


FIGURE 10 From top to bottom, distribution of the relative degree of polymerization a (A), crystallization b (B), the temperature T (C) at the end of the injection ( $t = 10 \text{ min}$ )

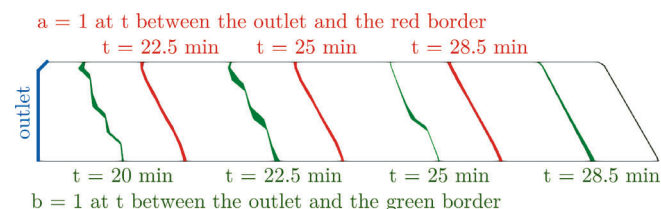


FIGURE 11 Proportion of the fully polymerized and fully crystallized part of the domain at different time, delimited between the outlet and the corresponding border

43.6% crystallinity that can be achieved in isothermal synthesis at 413 K. Moreover, the distribution of crystallinity at the end of the reaction seems to correspond to the temperature distribution in Figure 12D (the temperature scale was narrowed for visibility compared to Figure 12A,B). Because of the few elements where some colder and non-reacting air is left, it is near the outlet that the temperature is lower and the crystallinity higher. The crystallinity is also slightly higher at the core of the domain (near the symmetry border) because of the conduction of these lower temperature, which has less influence near the adiabatic borders. Therefore, the simulation gives some insights on how the synthesis can be affected by the injection. It creates a discrepancy on

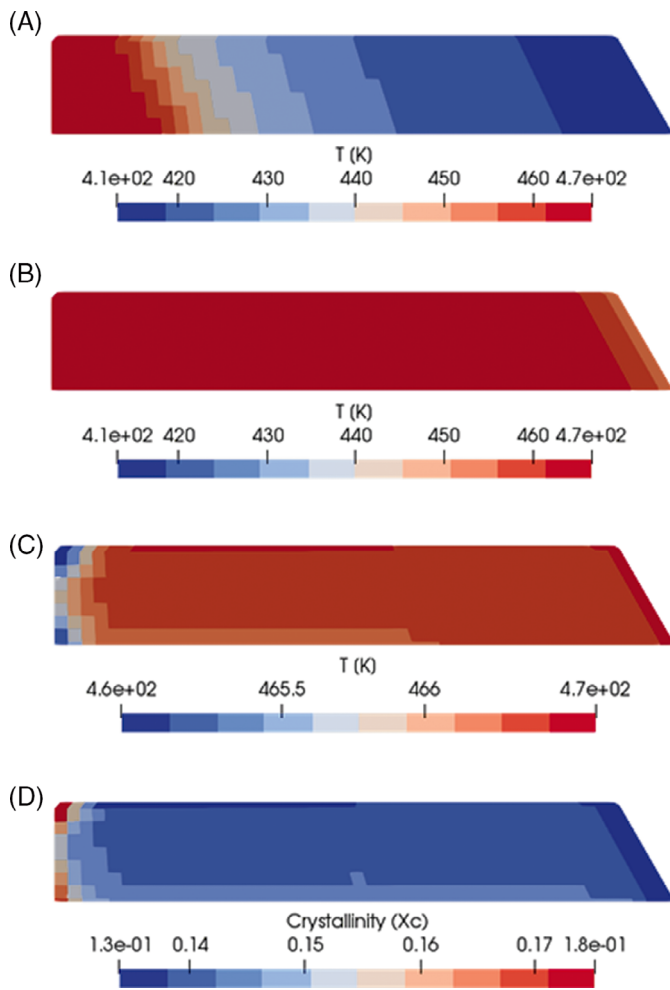


FIGURE 12 Temperature at (A)  $t = 20$  min, (B)  $t = 28.5$  min, (C)  $t = 30$  min and crystallinity (D) at  $t = 30$  min

the duration of the synthesis throughout the domain roughly equal to the injection duration, and on the crystallinity through the exothermy of the synthesis, which makes the reactive system hotter than the air present in the domain.

## 6 | CONCLUSION

In this work, a new coupling strategy has been formulated to simulate crystallization in an efficient way adapted for flow simulation of a reactive resin. It demonstrated its ability to describe the influence of the advancing polymerization on crystallization kinetics by considering the degree of crystallization relatively to the degree of polymerized chains ready to be crystallized.

Compared with the Gaussian separation method,<sup>[13–15]</sup> it offers a physical interpretation of the crystallization peak, while it corrects the inability of Bolgov et al. approach<sup>[17]</sup> to describe the PA6 synthesis

kinetics in a partially polymerized system.<sup>[21]</sup> Unlike Hillier's coupling, which considers that each polymer chain crystallizes independently, the new coupling method considers that there is a global crystallization kinetic that progresses depending on the polymerization state. These different physical interpretations were numerically confronted, and its nuances proved most important at temperatures when the phenomena occurred at similar time frames. However, the similar results given by these two approaches made us unable to distinguish the most likely or prevalent crystallization mechanism during the synthesis. Moreover, the need of a corrective factor to reduce the availability of the polymer chains for both models shows that a better understanding of the microscale initiation mechanisms of crystallization during polymerization is required.

The new coupling method showed its capacity in taking variability in measurement into account even without formally identifying its cause. Moreover, its differential form makes it highly suitable for methods based on spatial discretization, such as the finite volume method (FVM) or the finite element method (FEM). It was possible to integrate it in an Eulerian framework to consider the influence of the injection flow and the varying temperature during the synthesis on a macroscale. By updating the crystallization degree relatively to temperature, the potential effect of temperature difference caused by the exothermic synthesis was shown.

However, this effect needs to be confirmed with experimental studies. By comparing the coupling model to anisothermal DSC measurements, not only the simulated influence of anisothermal conditions on crystallinity can be confirmed, but more insights on observed variabilities can be determined and better understanding of the mesoscale mechanisms of the synthesis may be achieved.

On the other hand, the simulation relevancy at macroscale needs to be assessed by comparing it with a real injection in a fiber preform, notably by measuring the temperature and crystallinity. It will need to integrate the influence of permeability and varying flow at different scales and may allow confirmation of the simulation procedure or highlight the need for finer description of phenomena. Indeed, aside from the kinetic description improvement discussed above, other phenomena such as the shear stress can affect the polymerization speed while the varying density of the system throughout phases and temperatures may affect flow and the final shape of the composite.

## ACKNOWLEDGMENTS

The authors wish to thank the Occitanie region for its financial support.



## ABBREVIATIONS

DSC	differential scanning calorimetry
FVM	finite volume method
PA6	polyamide 6
RTM	resin transfer molding
SD	standard deviation

## INDEXES, EXPONENTS, AND DOT

$y_{i \in \{p,c,s\}}$	parameter $y$ relative to polymerization ( $p$ ), crystallization ( $c$ ), or the whole synthesis ( $s$ )
$y_{i \in \{r,g\}}$	parameter $y$ relative to the reactive mix phase ( $r$ ) or the air phase ( $g$ )
$y^\infty$	parameter $y$ at the end of a synthesis
$\dot{y}$	rate of parameter $y$ with regards to time during PA6 synthesis

## SYMBOLS

$R$	ideal gas constant
$T$	temperature
$H$	Heaviside function

## REACTION MONITORING PARAMETERS

$\varphi_{i \in \{p,c,s\}}$	heat flux of polymerization, crystallization, or the whole synthesis [ $\text{W g}^{-1}$ ]
$X_{i \in \{p,c\}}$	mass ratio of converted polymer or crystallinity
$\Delta H_{i \in \{p,c\}}^\infty$	total polymerization or crystallization enthalpy [ $\text{J g}^{-1}$ ]
$\Delta H_c^{100\%}$	theoretical crystallization enthalpy for 100% crystallinity [ $\text{J g}^{-1}$ ]
$Q$	reaction enthalpy [ $\text{J g}^{-1}$ ]
$Q_{\text{tot}}$	total reaction enthalpy [ $\text{J g}^{-1}$ ]
$t_{50\%}$	half-time of the synthesis [ $s$ ]
$a$	degree of polymerization progress
$b$	global degree of crystallization progress
$\beta$	local degree of crystallization progress

## SYNTHESIS MODEL PARAMETERS

$A_p$	pre-exponential factor
$E_a$	activation energy
$B_0$	autocatalytic factor
$n_p$	polymerization reaction order
$K_N$	Nakamura global kinetic constant
$n_c$	Avrami exponent representative crystals nucleation and growth
$U^*$	activation energy of macromolecular motion in the molten state
$K_0$	constant relative to molecular mass
$K_g$	constant relative to crystallization growth
$T_\infty$	limit temperature for macromolecular motion
$T_m^0$	equilibrium crystal melting temperature
$t_{c,0}$	crystallization induction time
$E_t$	activation energy for crystallization

$A_t$	pre-exponential factor for crystallization induction time
$f_d$	diffusion factor for polymer chains
$C, D$	diffusion factor parameters
$a_a$	degree of polymerization availability for crystallization

## OPTIMIZATION PARAMETERS

$Q_{\text{exp}}$	experimental enthalpy
$Q_{\text{sim}}$	simulated enthalpy
$\varphi_{\text{exp}}$	experimental heat flow
$\varphi_{\text{sim}}$	simulated heat flow
$a_i$	initial polymerization degree
$t_i$	polymerization induction time

## FLOW SIMULATION PARAMETERS


$\mathbf{u}$	flow velocity vector
$\mathbf{u}_i \in \{r,g\}$	phase $i$ velocity vector at the interface
$p$	pressure
$\eta$	mixed dynamic viscosity
$\rho$	mixed density
$\alpha_i \in \{r,g\}$	phase $i$ volume fraction
$\Delta t$	time step
$\Delta l$	element characteristic length

## HEAT EQUATION PARAMETERS

$\dot{q}$	heat equation source term
$c_p$	mixed specific heat capacity
$\kappa$	mixed thermal conductivity

## ORCID

William Han  <https://orcid.org/0000-0002-4177-1915>

Quentin Govignon  <https://orcid.org/0000-0003-0971-0845>

Arthur Cantarel  <https://orcid.org/0000-0002-3653-6515>

Fabrice Schmidt  <https://orcid.org/0000-0002-0678-2133>

## REFERENCES

- [1] K. van Rijswijk, H. E. N. Bersee, *Compos. Part A Appl. Sci. Manuf.* **2007**, 38, 666.
- [2] T. Ishikawa, K. Amaoka, Y. Masubuchi, T. Yamamoto, A. Yamanaka, M. Arai, J. Takahashi, *Compos. Sci. Technol.* **2018**, 155, 221.
- [3] O. Wichterle, J. Šebenda, J. Králíček, *Adv. Polym. Sci.* **1961**, 2, 578.
- [4] T. Kōmoto, M. Iguchi, H. Kanetsuna, T. Kawai, *Makromol. Chem.* **1970**, 135, 145.
- [5] C. Vicard, O. De Almeida, A. Cantarel, G. Bernhart, *Polymer* **2017**, 132, 88.
- [6] H. Tan, K. M. Pillai, *Compos. Part Appl. Sci. Manuf.* **2012**, 43, 29.
- [7] L. Zingraff, V. Michaud, P.-E. Bourban, J.-A. E. Månson, *Compos. Part Appl. Sci. Manuf.* **2005**, 36, 1675.
- [8] E. Abisset-Chavanne, F. Chinesta, *Int. J. Mater. Form.* **2014**, 7, 249.



- [9] J. Nagy, L. Reith, M. Fischlschweiger, G. Steinbichler, *Chem. Eng. Sci.* **2014**, *111*, 85.
- [10] M. Imbert, E. Abisset-Chavanne, S. Comas-Cardona, D. Prono, *J. Compos. Mater.* **2018**, *52*, 313.
- [11] W. Han, Q. Govignon, A. Cantarel, C. Samuel, F. Schmidt, ESAFORM 2021 2021. <https://doi.org/10.25518/esaform21.4351>
- [12] R. Spina, M. Spekowius, C. Hopmann. 2013 COMSOL Conf. **2013**.
- [13] J. Karger-Kocsis, L. Kiss, *Makromol. Chem.* **1979**, *180*, 1593.
- [14] K. Taki, N. Shoji, M. Kobayashi, H. Ito, *Microsyst. Technol.* **2017**, *23*, 1161.
- [15] J. Humphry, N. Yang, L. J. Vandi, B. V. Hernandez, D. J. Martin, M. T. Heitzmann, *Mater. Today Commun.* **2020**, *25*, 101473.
- [16] V. V. Korshak, T. M. Frunze, S. P. Davtyan, V. V. Kurashev, T. V. Volkova, V. A. Kot'elnikov, R. B. Shleifman, *Polym. Sci. USSR* **1979**, *21*, 2161.
- [17] S. A. Bolgov, V. P. Begishev, A. Y. Malkin, V. G. Frolov, *Polym. Sci. USSR* **1981**, *23*, 1485.
- [18] A. Y. Malkin, V. P. Beghishev, S. A. Bolgov, *Polymer* **1982**, *23*, 385.
- [19] K. H. Lee, S. C. Kim, *Polym. Eng. Sci.* **1988**, *28*, 8.
- [20] J. J. E. Teuwen, A. A. van Geenen, H. E. N. Bersee, *Macromol. Mater. Eng.* **2013**, *298*, 163.
- [21] C. Vicard, O. De Almeida, A. Cantarel, G. Bernhart, *Polymer* **2019**, *180*, 121681.
- [22] I. H. Hillier, *J. Polym. Sci. A* **1965**, *3*, 3067.
- [23] J. Fournier, G. Williams, C. Duch, G. A. Aldridge, *Macromolecules* **1996**, *29*, 7097.
- [24] K. Ueda, K. Yamada, M. Nakai, T. Matsuda, M. Hosoda, K. Tai, *Polym. J.* **1996**, *28*, 6.
- [25] M. Wilhelm, R. Wendel, M. Aust, P. Rosenberg, F. Henning, *J. Compos. Sci.* **2020**, *4*, 7.
- [26] C. Vicard. Ph.D. Thesis, Ecole des Mines d'Albi-Carmaux. 2018.
- [27] S. Pillay, U. K. Vaidya, G. M. Janowski, *J. Thermoplast. Compos. Mater.* **2005**, *18*, 509.
- [28] R. E. Camargo, V. M. Gonzalez, C. W. Macosko, M. Tirell, *Rubber Chem. Technol.* **1983**, *56*, 774.
- [29] K. Nakamura, K. Katayama, T. Amano, *J. Appl. Polym. Sci.* **1973**, *17*, 1031.
- [30] M. Avrami, *J. Chem. Phys.* **1940**, *8*, 212.
- [31] J. D. Hoffman, J. I. Lauritzen, *J. Res. Natl. Bur. Stand. Sect. Phys. Chem.* **1961**, *65A*, 297.
- [32] J. Magill, *Polymer* **1962**, *3*, 655.
- [33] I. Kolesov, D. Mileva, R. Androsch, C. Schick, *Polymer* **2011**, *52*, 5156.
- [34] C. Schick, V. Mathot, *Fast Scanning Calorimetry*, 1st. ed., Springer International Publishing, Switzerland **2016**. <https://doi.org/10.1007/978-3-319-31329-0>
- [35] R. M. Patel, J. E. Spruiell, *Polym. Eng. Sci.* **1991**, *31*, 730.
- [36] O. Wichterle, J. Šebenda, J. Tomka, *J. Polym. Sci.* **1962**, *57*, 785.
- [37] J. J. E. Teuwen, Ph.D. Thesis, Technische Universiteit Delft **2011**.
- [38] R. Wendel, P. Rosenberg, M. Wilhelm, F. Henning, *J. Compos. Sci.* **2020**, *4*, 8.
- [39] K. van Rijswijk, H. E. N. Bersee, W. F. Jager, S. J. Picken, *Compos. Part Appl. Sci. Manuf.* **2006**, *37*, 949.
- [40] K. E. Wardle, H. G. Weller, *Int. J. Chem. Eng.* **2013**, *2013*, 1.
- [41] R. S. Davé, L. Kruse, *Polymer* **1997**, *38*, 949.
- [42] A. Levy, *Int. J. Theor. Appl. Math.* **2017**, *3*, 143.
- [43] R. I. Issa, A. D. Gosman, A. P. Watkins, *J. Comput. Phys.* **1986**, *62*, 66.
- [44] B. van Leer, *J. Comput. Phys.* **1974**, *14*, 361.